# RLx2: Training a Sparse Deep Reinforcement Learning Model from Scratch

Yiqin Tan\*, Pihe Hu; Ling Pan, Longbo Huang

Institute for Interdisciplinary Information Sciences (IIIS)

Tsinghua University

Beijing, China

{tanyq18, hph19, pl17}@mails.tsinghua.edu.cn, longbohuang@tsinghua.edu.cn

#### **Abstract**

Training deep reinforcement learning (DRL) models usually requires high computation costs. Therefore, compressing DRL models possesses immense potential for training acceleration and model deployment. However, existing methods that generate small models mainly adopt the knowledge distillation based approach by iteratively training a dense network, such that the training process still demands massive computing resources. Indeed, sparse training from scratch in DRL has not been well explored and is particularly challenging due to non-stationarity in bootstrap training. In this work, we propose a novel sparse DRL training framework, "the Rigged Reinforcement Learning Lottery" (RLx2), which is capable of training a DRL agent using an ultra-sparse network throughout for off-policy reinforcement learning. The systematic RLx2 framework contains three key components: gradient-based topology evolution, multi-step Temporal Difference (TD) targets, and dynamic-capacity replay buffer. RLx2 enables efficient topology exploration and robust Q-value estimation simultaneously. We demonstrate state-of-the-art sparse training performance in several continuous control tasks using RLx2, showing  $7.5 \times -20 \times$  model compression with less than 3% performance degradation, and up to  $20 \times$  and  $50 \times$  FLOPs reduction for training and inference, respectively.

#### 1 Introduction

Deep reinforcement learning (DRL) has found successful applications in many important areas, e.g., games [35], robotics[14] and nuclear fusion [6]. However, training a DRL model demands heavy computational resources. For instance, AlphaGo-Zero for Go games [35], which defeats all Go-AIs and human experts, requires more than 40 days of training time on four tensor processing units (TPUs). The heavy resource requirement hinders the application of DRL on resource-limited devices and results in expensive consumption.

Sparse networks, initially proposed in deep supervised learning, have demonstrated great potential for model compression and training acceleration of deep reinforcement learning. In deep supervised learning, the state-of-the-art sparse training frameworks, e.g., SET [26] and RigL [10], can train a 90%-sparse network (i.e., the resulting network size is 10% of the original network) from scratch without performance degradation. Existing works [32, 33, 44] also attempt to compress DRL models using knowledge distillation. The lottery ticket hypothesis (LTH) [12], which claims the existence of a good fixed sparse network (a.k.a. the "winning ticket") in deep supervised learning, is also observed in [43] to be useful for DRL compression. It is further shown in [41] that a "winning ticket" achieves high sparsity levels of 90% by behavioral cloning (BC). However, we note that the results mentioned above mainly focus on generating an ultimately small network and are based

<sup>\*</sup>Equal Contribution

on knowledge distillation or supervised learning type methods. Thus, they still require iteratively training a dense network, e.g., due to the need to pre-train dense teachers. As a result, the training cost remains prohibitively high, and the methods cannot be directly implemented on resource-limited devices, leading to low flexibility in adapting the compressed models to new environments.

Training a sparse DRL model from scratch, if done perfectly, has the potential to significantly reduce computation expenditure and enable efficient implementation on resource-limited devices, and achieves excellent flexibility in model adaptation. However, training a sparse network (e.g., 90% sparsity) from scratch in DRL is challenging due to the non-stationarity in bootstrap training. Specifically, in DRL, the learning target is not fixed but evolves in a bootstrap way (i.e., TD target) [39], and the distribution of the training data can also be non-stationary [7]. Moreover, using a sparse network structure means searching in a smaller hypothesis (topology) space, which further reduces the learning target's confidence. As a result, improper sparsification can cause irreversible damage to the learning path [21], resulting in poor performance. Indeed, it is shown in [36] that a direct adoption of a dynamic sparse training framework in DRL, i.e., SET in TD3, can only compress the model by a half (50% sparsity) without much performance degradation. This result indicates the significant performance gap between training from scratch and using knowledge distillation and BC [41], and raises the following interesting open question:

Can an efficient DRL agent be trained from scratch with an ultra-sparse network throughout?

In this paper, we give an affirmative answer to the problem and propose a novel sparse training framework, "the Rigged Reinforcement Learning Lottery" (RLx2), for off-policy RL. RLx2 is motivated by our observation that topology evolution and accurate value estimation are two critical steps in training DRL from scratch. As an illustrating experiment, Fig. 1 presents a comparison on Ant-v3, one of Mu-JoCo [40] environments, for four methods generating sparse networks for DRL under different sparsity <sup>2</sup>, including a small dense network (Tiny Dense, orange), a fixed sparse network (Static Sparse, green), a dynamic-structure training scheme without accurate value estimation (Topology Evolution, red), and RLx2 (purple). The result indicates that both topology evolution and accurate value estimation are indispensable. In particular, we apply a gradient-guided topology search scheme [10] to enable dynamic network evolution. We further equip

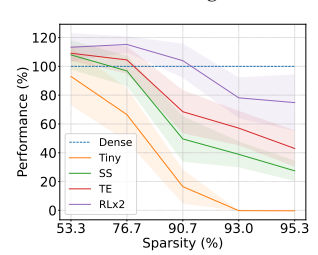


Figure 1: Comparison of four methods with TD3 on Ant-v3 under different sparsity. The performance is normalized to that of the original dense model.

RLx2 with multi-step temporal difference (TD) targets for more accurate value estimation, with a novel dynamic-capacity replay buffer for correcting the off-policy issue. These three key steps simultaneously achieve efficient topology exploration and better value estimates in sparse models. Through extensive experiments in various environments using RLx2 with two popular off-policy RL algorithms, TD3 and SAC, we demonstrate that RLx2 is able to achieve superb model compression with minimal performance degradation by *using an ultra-sparse network throughout training*. We summarize the main contributions of the paper as follows.

- We conduct an in-depth investigation on the obstacles to training a sparse neural network from scratch in DRL, and discover two key ingredients necessary for success, namely topology evolution and accurate value estimation.
- We propose RLx2, a novel sparse training framework for DRL. RLx2 consists of a gradient-guided topology search scheme, which dynamically grows and deletes network connections with magnitude and value-based gradient criteria and a multi-step Temporal Difference (TD) target and dynamic-capacity replay buffer to handle data inconsistency and improve the value estimation. RLx2 simultaneously achieves efficient topology exploration in the reduced search space, which enables model compression, and accurate value estimation, which guarantees performance.
- We demonstrate the state-of-the-art sparse training performance of RLx2 with two popular off-policy RL algorithms, TD3 [13] and SAC [16], in various environments. The extensive experimental results demonstrate up to 20× model compression, even better than the current

<sup>&</sup>lt;sup>2</sup>Here sparsity equals to  $(1-r) \times 100\%$ , where r is the fraction of model size reduced (detailed in Appendix). For instance, a sparse model whose size is 10% of the original model has a 90% sparsity.

best sparsity obtained based on BC in [41]. RLx2 also achieves  $20 \times$  acceleration in training and  $50 \times$  in inference in floating-point operations (FLOPs).

#### 2 Related Works

We discuss the related works on training sparse models in deep supervised learning and reinforcement learning below. We also provide a comprehensive performance comparison in Table 1.

Sparse Models in Deep Supervised Learning [18, 17, 37, 45] focus on finding a sparse network by pruning pre-trained dense networks. Iterative Magnitude Pruning (IMP) in [17] achieves a sparsity of more than 90%. Neuron characteristic [20], dynamic network surgery [15], derivatives [9, 29], regularization [25, 38], dropout [27] have also been applied in network pruning. Another line of work focus on the Lottery Ticket Hypothesis (LTH), first proposed in [12], which shows that training from a sparse network from scratch is possible if one finds a sparse "winning ticket" initialization in deep supervised learning. The LTH is also validated in other deep learning models [4, 3, 5]. Many works [2, 26, 30, 8, 10] also try to train a sparse neural network from scratch without having to pre-trained dense models. These works adjust structures of sparse networks during training, including Deep Rewiring (DeepR) [2], Sparse Evolutionary Training (SET) [26], Dynamic Sparse Reparameterization (DSR) [30], Sparse Networks from Scratch (SNFS) [8], and Rigged Lottery (RigL) [10]. On the contrary, Single-Shot Network Pruning (SNIP) [23] and Gradient Signal Preservation (GraSP) [42] focus on finding static sparse networks before training begins.

Table 1: Comparison of different sparse training techniques in DRL. Here ST and TA stand for "sparse throughout training" and "training acceleration," respectively. The shown sparsity is the maximum sparsity level without performance degradation under the algorithms.

Name	Paradigm	Scenario	ST	TA	benchmark	Sparsity
PoPS [24]	IMP	Online	No	No	Atari	$\sim 99\%$
LTH-RL [43]	IMP	Online	Yes	No	Atari	$\sim 99\%$
LTH-IL [41]	IMP	Online	Yes	No	PyBullet,etc.	$\sim 95\%$
SSP [1]	Single-shot pruning	Offline	Yes	Yes	MuJoCo	$\sim 95\%$
GST [22]	Gradual pruning	Online	No	No	MuJoCo	$\sim 70\%$
DST [36]	Topology Evolution	Online	Yes	Yes	MuJoCo	$\sim 50\%$
RLx2 (Ours)	Topology Evolution	Online	Yes	Yes	MuJoCo	$\sim 95\%$

**Sparse Models in DRL** [10, 36] show that finding a sparse model in DRL is difficult due to training instability. Existing works [32, 33, 44] leverage knowledge distillation to avoid unstable training and obtains small dense agents. Policy Pruning and Shrinking (PoPs) in [24] obtains a sparse DRL agent with iterative policy pruning (similar to IMP). LTH in DRL is investigated in [43]. [41] shows that a sparse winning ticket can be found by behavior cloning (BC). Another line of works [22, 36, 1] attempts to train a sparse neural network from scratch without pre-training a dense teacher. Group Sparse Training (GST) in [22] utilizes block-circuit compression and reward-aware pruning. [36] proposes using SET in topology evolution in DRL and achieves 50% sparsity. [1] proposes single-shot pruning (SSP) for offline RL.

#### 3 Deep Reinforcement Learning Preliminaries

In reinforcement learning, an agent interacts with an unknown environment to learn an optimal policy. The learning process is formulated as a Markov decision process (MDP)  $\mathcal{M} = \langle \mathcal{S}, \mathcal{A}, r, \mathbb{P}, \gamma \rangle$ , where  $\mathcal{S}$  is the state space,  $\mathcal{A}$  is the action space, r is the reward function,  $\mathbb{P}$  denotes the transition matrix, and  $\gamma$  stands for the discount factor. Specifically, at time slot t, given the current state  $s_t \in \mathcal{S}$ , the agent selects an action  $a_t \in \mathcal{A}$  by policy  $\pi : \mathcal{S} \to \mathcal{A}$ , which then incurs a reward  $r_t(s, a)$ .

Denote the Q function associated with the policy  $\pi$  for state-action pair (s, a) as

$$Q_{\pi}(s, a) = \mathbb{E}_{\pi} \left[ \sum_{i=t}^{T} \gamma^{i-t} r(s_i, a_i) | s_t = s, a_t = a \right].$$
 (1)

In actor-critic methods [34], the policy  $\pi(s;\phi)$  is parameterized by a policy (actor) network with weight parameter  $\phi$ , and the Q function  $Q(s,a;\theta)$  is parameterized by a value (critic) network with parameter  $\theta$ . The goal of the agent is to find an optimal policy  $\pi^*(s;\phi^*)$  which maximizes long-term cumulative reward, i.e.,  $J^* = \max_{\phi} \mathbb{E}_{\pi(\phi)}[\sum_{i=t}^T \gamma^{i-t} r(s_i,a_i)|s_0,a_0]$ .

There are various DRL methods for learning an efficient policy. In this paper, we focus on off-policy TD learning methods, including a broad range of state-of-the-art algorithms, e.g., TD3 [13] and SAC [16]. Specifically, the critic network is updated by gradient descent to fit the TD targets  $\mathcal{T}_1(s_t, a_t)$  generated by a target network  $Q(s, a; \theta')$ , i.e.,

$$\mathcal{T}(s_t, a_t) = r(s_t, a_t) + \gamma Q(s_{t+1}, a_{t+1}; \theta')$$
(2)

for state-action pair  $(s_t, a_t)$  at time slot t, where the action  $a_t = \pi(s_t; \phi)$ . The loss function of the value network is defined as the expected squared loss between current value network and TD targets:

$$\mathcal{L}(\theta) = \mathbb{E}_{\pi(\phi)} \left[ Q(s_i, a_i; \theta) - \mathcal{T} \right]^2. \tag{3}$$

The policy  $\pi(s;\phi)$  is updated by the deterministic policy gradient algorithm in [34] as

$$\nabla_{\phi} J(\phi) = \mathbb{E}_{\pi(\phi)} \left[ \left. \nabla_{a} Q(s, a; \theta) \right|_{a = \pi(s; \phi)} \nabla_{\phi} \pi(s; \phi) \right].$$

## 4 RLx2: Rigging the Lottery in DRL

We introduce our RLx2 algorithm in this section. First, we compare sparse DRL training methods using TD3 with different topology update schemes on InvertedPendulum-v2, a simple control task from MuJoCo [40], in Figure 2. From the results, we make the following important observations. First, dynamic topology evolution is crucial. This can be seen from the fact that a random static sparse network (SS, orange) does not achieve a satisfying performance and performs much worse than that with topology evolution (TE, green). Second, accurate value estimation is essential. Unlike supervised learning, DRL training heavily relies on value estimation. Thus, improving the value estimation can intuitively boost the learning performance. This is confirmed by the comparison between TE and TE+ $Q^*$  (purple), which is an ideal scheme using topology evolution (same as in TE) yet replacing TD targets with expert Q-values, i.e., Q-values from a fully trained expert critic with a dense network. Our RLx2 algorithm, which contains both topology evolution [10] (using the same scheme in TE) and accurate value estimation (using multi-step TD targets [19]), is able to achieve a performance close to TE+ $Q^*$  without the need for pre-trained expert Q-values.

These results clearly demonstrate that both topology evolution and accurate value estimation are critical for training a sparse DRL agent from scratch.

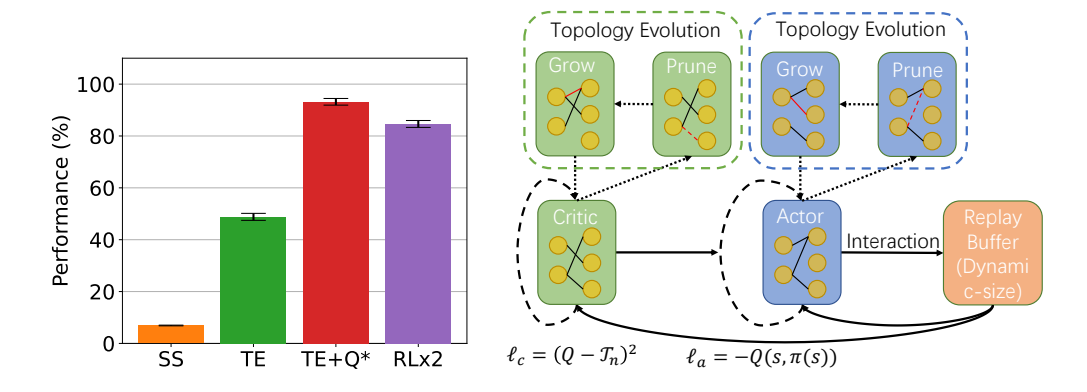


Figure 2: Performance of sparse DRL agents obtained under different methods.

An overview of RLx2 on an actor-critic architecture is shown in Figure 3. Below, we will explain the key components of RLx2 in detail, including topology evolution, multi-step TD target, and dynamic-capacity buffer.

Figure 3: Overview of RLx2.

#### 4.1 Topology Evolution

The topology evolution in RLx2 is made by adopting the RigL [10] method. Specifically, we compute the gradient values of the loss function with respect to each link weight. Then, we dynamically grow connections (connecting neurons) with large gradients and delete existing links with the least weights. In this way, we obtain a sparse mask that evolves by self-adjustment. Please refer to [10] for more details.

The pseudo-code of our scheme is given in Algorithem 1, where ⊙ is an element-wise multiplication operator and  $M_{\phi}$  is a binary mask to represent the sparse architecture of the network  $\phi$ . The update fraction anneals during the training process as  $\zeta_t = \frac{\zeta_0}{2}(1 + \cos(\frac{\pi t}{T_{\rm end}}))$ , where  $\zeta_0$  is the initial update fraction and  $T_{\rm end}$  is the total number of iterations.

Adopting the RigL scheme in deep reinforcement learning can have more profound implications. Due to the potential data inconsistency problem in value estimation and the smaller hypothesis search space under sparse networks, training with a single fixed topology does not fully reap the benefit of a sparse topology and can result in significantly degraded performance. Please see further discussion on this in Section 5.3.

#### **Algorithm 1** Topology Evolution [10]

- 1:  $N_l$ : Number of parameters in layer l
- 2:  $\theta_l$ : Parameters in layer l
- 3:  $M_{\theta_l}$ : Sparse mask of layer l
- 4:  $s_l$ : Sparsity of layer l
- 5: L: Loss function
- 6:  $\zeta_t$ : Update fraction in training step t
- 7: **for** each layer l **do**

- $\begin{array}{lll} & k = \zeta_t(1-s_l)N_l \\ 9: & \mathbb{I}_{\text{drop}} = \text{ArgTopK}(-|\theta_l \odot M_{\theta_l}|, k) \\ 10: & \mathbb{I}_{\text{grow}} = \text{ArgTopK}_{i \notin \theta_l \odot M_{\theta_l} \setminus \mathbb{I}_{\text{drop}}}(|\nabla_{\theta_l} L, k|) \\ 11: & \text{Update } M_{\theta_l} \text{ according to } \mathbb{I}_{\text{drop}} \text{ and } \mathbb{I}_{\text{grow}} \end{array}$
- 12:  $\theta_l \leftarrow \theta_l \odot M_{\theta_l}$
- 13: **end for**

#### Accurate Value Learning 4.2

As discussed above, the learning of the value function is crucial in sparse training. It not only serves to guarantee the efficiency of the DRL agent but also guides the adjustment of the sparse network during training. To achieve accurate value estimation, RLx2 utilizes two components, including a multi-step TD target to bootstrap value estimation, and a dynamic-capacity replay buffer to eliminate the potential data-inconsistency problem due to policy change during training.

#### 4.2.1 Multi-step TD Target

In TD learning, a TD target is generated to update the value network by minimizing the squared loss concerning the TD target. Single-step methods generate the TD target by one-step reward and discounted target network output, i.e.,

$$\mathcal{T}_1 = r_t + \gamma Q(s_{t+1}, \pi(s_{t+1}); \theta) \tag{4}$$

However, a sparse network  $\widehat{\theta}=\theta\odot M_{\theta}$ , obtained from  $\theta$ , inevitably contains only a smaller hypothesis space compared to a dense network, which means the output of the sparse value network  $\hat{\theta}$  can be unreliable and lead to inaccurate value estimation. Denote the network fitting error as  $\epsilon(s,a) = Q(s,a;\theta) - Q_{\pi}(s,a)$ . We see that this error can be non-negligible when the sparsity of the value network is relatively high in Eq. (4).

To overcome this issue, we introduce multi-step targets in Eq. (5), where the target combines an N-step sample and the output of the sparse value network with reduced weight.

$$\mathcal{T}_n = \sum_{k=0}^{n-1} \gamma^k r_{t+k} + \gamma^n Q(s_{t+n}, \pi(s_{t+n}); \theta)$$
 (5)

By doing so, we reduce the expected error between the TD target and the real target. Specifically, Eq.(6) shows the expected TD error between multi-step TD target  $\mathcal{T}_n$  and the real Q function  $Q_{\pi}$ associated with the target policy  $\pi$  conditioned on transitions from behavior policy b (see detailed derivation in Appendix).

$$\mathbb{E}_{b}[\mathcal{T}_{n}(s,a)] - Q_{\pi}(s,a) = \underbrace{\left(\mathbb{E}_{b}[\mathcal{T}_{n}(s,a)] - \mathbb{E}_{\pi}[\mathcal{T}_{n}(s,a)]\right)}_{\text{Policy inconsistency error}} + \gamma^{n} \underbrace{\mathbb{E}_{\pi}[\epsilon(s_{n},\pi(s_{n}))]}_{\text{Network fitting error}}$$
(6)

Eq.(6) shows that the expected error consists of two parts, i.e., the policy inconsistency error and network fitting error. In particular, introducing a multi-step target reduces the network fitting error by a reduced weight  $\gamma^n$ . However, it has been observed, e.g., in [11], that a immediate adoption of multi-step TD targets may enlarge the policy inconsistency error (the first term). To suppress the policy inconsistency and further improve value learning, we introduce a novel adaptive scheme to control the replay buffer capacity to eliminate data inconsistency (detailed in Section 4.2.2 below).

#### 4.2.2 Dynamic-capacity Buffer

Off-policy algorithms use a replay buffer to store collected data and train networks with sampled batches from the buffer, and their performance generally improves with increased replay capacity [11]. However, off-policy algorithms with unlimited-size replay buffers can suffer from policy inconsistency due to inconsistent multi-step targets and mismatched training data, which we discuss below.

- (i) Inconsistent multi-step targets: In off-policy algorithms with multi-step TD targets, the value function is updated to minimize the squared loss in Eq. (3) by sampling transitions in replay buffer, i.e., reward sequence  $r_t, r_{t+1}, \cdots, r_{t+n}$  collected during training. However, the fact that the policy can evolve during training means the data in the replay buffer, which is used to form Monte-Carlo approximation of the current policy  $\pi$ , may be collected with a different behavior policy b. As a result, the policy inconsistency error in Eq. (6 may be enlarged, leading to inaccuracy estimation.
- (ii) Mismatched training data: In practice, the agent minimizes the value loss  $\widehat{\mathcal{L}}(\theta)$  with respect to the sampled value of mini-batch  $\mathcal{B}_t$ , which is given as

$$\widehat{\mathcal{L}}(\theta) = \frac{1}{|\mathcal{B}_t|} \sum_{(s_i, a_i) \sim \mathcal{B}_t} (Q(s_i, a_i; \theta) - \mathcal{T})^2$$
(7)

Compared to Eq. (3, the difference between the distribution of transitions in the mini-batch  $\mathcal{B}_t$  and that of current policy also leads to a mismatch.

The off-policy issue may be exacerbated by sparse training due to using smaller models. To tackle these issues, we propose a dynamic-capacity buffer to reduce the policy gap based on the policy distance of the collected data. The formal scheme is given in Algorithm 2. Specifically, we introduce the following policy distance measure to evaluate the inconsistency of data in the buffer, i.e.,

$$\mathcal{D}(\phi) = \frac{1}{|\mathcal{B}_0|} \sum_{(s_i, a_i) \in \mathcal{B}_0} \| \pi(s_i; \phi) - a_i \|_2$$
 (8)

where  $\mathcal{B}_0$  denotes the oldest mini-batch of the replay buffer and  $\pi$  is the current policy. If this measure is below a certain pre-specified threshold, we enlarge the buffer. Otherwise, we replace the oldest data with the newly collected samples.

#### 5 Experiments

In this section, we conduct an extensive evaluation to investigate the performance improvement of RLx2, and investigate the importance of each component in RLx2. We further analyze the differences between the dynamic network topology and a winning ticket. Specifically, we conduct extensive experiments on four MuJoCo environments: HalfCheetah-v3 (Hal.), Hopper-v3 (Hop.), Walker2d-v3 (Wal.), and Ant-v3 (Ant.), for our proposed sparse training framework RLx2 with two off-policy algorithms, TD3 and SAC. Instantiations of RLx2 on TD3 and SAC are provided in Appendix. Each result is averaged over eight random seeds.

#### 5.1 Comparative Evaluation

We first present a comparative evaluation of RLx2 with TD3 and SAC on four MuJoCo environments in Table 2. In our experiments, we compare RLx2 with the following baselines: (i) Tiny, which uses tiny dense networks with the same number of parameters as the sparse model in training. (ii) SS: using static sparse networks with random initialization. (iii) SET [2], which uses dynamic sparse training by dropping connections with magnitude criteria and growing connections randomly. (iv)

RigL [10], which uses dynamic sparse training by dropping and growing connections with magnitude and gradient criteria, respectively, the same as RLx2's topology evolution procedure.

In our experiments, we allow the actor and critic networks to take different sparsities. We define an ultimate compression ratio, i.e., the largest sparsity level ensuring that the performance degradation under RLx2 is within  $\pm\%3$  of that under the original dense models. This can also be understood as the minimum size of the sparse model with the full performance of the original dense model. We present performance comparison results in Table 2 based on the ultimate compression ratio. The performance of each algorithm is evaluated with the average reward per episode over the last 30 evaluations of the training (evaluation is conducted every 5000 steps). Hyperparameters are fixed in all four environments for TD3 and SAC, respectively, which are presented in Appendix.

Table 2: Comparisons of RLx2 with sparse training baselines. Here "Sp." refers to the sparsity level (percentage of model size reduced), "Total Size" refers to the total parameters of both critic and actor networks (detailed calculation of training and inference FLOPs are given in Appendix). The right five columns show the final performance of different methods. The "Total size," "FLOPs", and "Performance" are all normalized w.r.t. the original large dense model (detailed in Appendix).

Alg.	Env.	Actor Sp.	Critic Sp.	Total Size	FLOPs (Train)	FLOPs (Test)	Tiny (%)	SS (%)	SET (%)	RigL (%)	RLx2 (%)
TD3	Hal. Hop. Wal. Ant.	90% 98% 97% 96%	85% 95% 95% 88%		0.043x 0.045x	0.100x 0.020x 0.030x 0.040x	86.3 64.5 60.8 16.5	77.1 67.7 42.9 49.6	92.6 66.5 39.3 62.5	90.8 90.6 35.7 68.5	99.8 97.0 98.1 103.9
	Avg.	95%	91%	0.077x	0.082x	0.048x	57.0	59.3	65.2	71.4	99.7
SAC	Hal. Hop. Wal. Ant	90% 98% 90% 90%	80% 95% 90% 75%	0.180x 0.044x 0.100x 0.220x	0.043x 0.107x	0.100x 0.020x 0.100x 0.100x	95.0 89.1 73.8 49.6	75.4 81.6 83.4 49.3	94.8 103.9 95.8 79.8	89.8 <b>110.0</b> 81.9 90.9	102.2 109.7 103.2 105.6
	Avg.	92%	85%	0.136x	0.136x	0.080x	76.9	72.4	93.6	93.2	105.2
A	vg.	94%	88%	0.107x	0.109x	0.064x	67.0	65.9	79.4	82.3	102.4

From Table 2, we see that RLx2 achieves superior compression ratios (the reciprocal of the total size) compared to others. Specifically, RLx2 with TD3 achieves  $7.5 \times -25 \times$  model compression, with the best compression ratios of  $25 \times$  on Hopper-v3. The actor can be compressed for each environment by more than 96% and the critic is compressed by 85%-95%. The results for SAC are similar. RLx2 with SAC achieves a  $5 \times -20 \times$  model compression. In addition to the superior compression performance, RLx2 also performs best among all baselines in all four environments (except for a close performance with RigL with SAC in Hopper) by a large margin, which validates the state-of-the-art performance of our RLx2 framework in model compression, training, and inference acceleration.

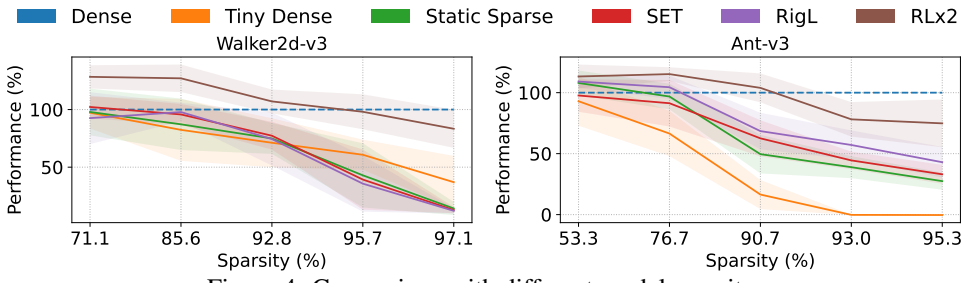


Figure 4: Comparison with different model sparsity.

Tiny dense (Tiny) and random static sparse networks (SS) performance are worst on average. SET and RigL are better yet fail to maintain the performance in Walker2d-v3 and Ant-v3, which means robust value learning is necessary under sparse training. We want to highlight here that different from knowledge-distillation/BC based methods, e.g., [24, 41, 22], RLx2 uses a sparse network throughout training. Thus, it has an additional advantage of immensely accelerating training and saving computation, i.e.,  $12\times$  training acceleration and  $20\times$  inference acceleration for RLx2-TD3, and  $7\times$  training acceleration and  $12\times$  inference acceleration for RLx2-SAC. To further validate

the performance of RLx2, we compare the performance of RLx2-TD3 with other baselines under different sparsity levels in Hopper-v3 and Ant-v3 in Figure 4. We find that RLx2 has a significant performance gain over other baselines.

#### 5.2 Ablation Study

We conduct a comprehensive ablation study on three critical components of RLx2 on TD3, i.e., topology evolution, multi-step TD target, and dynamic-capacity buffer, to examine the effect of each component in RLx2 and their robustness in hyperparameters.

**Topology evolution** RLx2 drops and grows connections with magnitude and gradient criteria, respectively, which has been adopted in RigL [10] for deep supervised learning. To validate the necessity of our topology evolution criteria, we compare RLx2 with three baselines, which replace the topology evolution scheme in RLx2 with Tiny, SS and SET, with other components in RLx2 remain unchanged, i.e., they are also equipped with multi-step targets and dynamic-capacity buffer.

The left part of Table 3 shows that RigL as a topology adjustment scheme (Note that in this case, the scheme is RLx2) performs best on average among four baselines. We also observe that Tiny performs worst, which is consistent with the conclusion in existing works [45] that a sparse network may contain a smaller hypothesis space and necessitates a topology evolution scheme.

Table 3: Ablation study on topology evolution and multi-step target, where the performance (%) is normalized with respect to the performance of dense models.

Env.	Topoloy Evolution			Multi-step Target					
	Tiny	SS	SET	RLx2	1-step	2-step	3-step	4-step	5-step
Hal.	93.3	86.1	100.1	99.8	96.5	101.7	99.8	98.8	97.0
Hop.	74.4	84.2	88.8	97.0	77.9	91.7	97.0	84.0	87.5
Wal.	84.1	83.8	89.4	98.1	73.9	93.7	98.1	99.1	99.3
Ant.	28.7	80.2	83.5	103.9	103.9	105.1	103.9	96.7	94.5
Avg.	70.1	83.6	90.4	99.7	88.1	98.1	99.7	94.6	94.6

**N-step TD target** We also compare different step lengths in multi-step TD targets for RLx2 in the right part of Table 3. We find that multi-step TD targets with step length 3 obtain the maximum performance. In particular, multi-step TD targets improve the performance dramatically in Hopper-v3 and Walker2d-v3, while the improvement in HalfCheetach-v3 and Ant-v3 is minor.

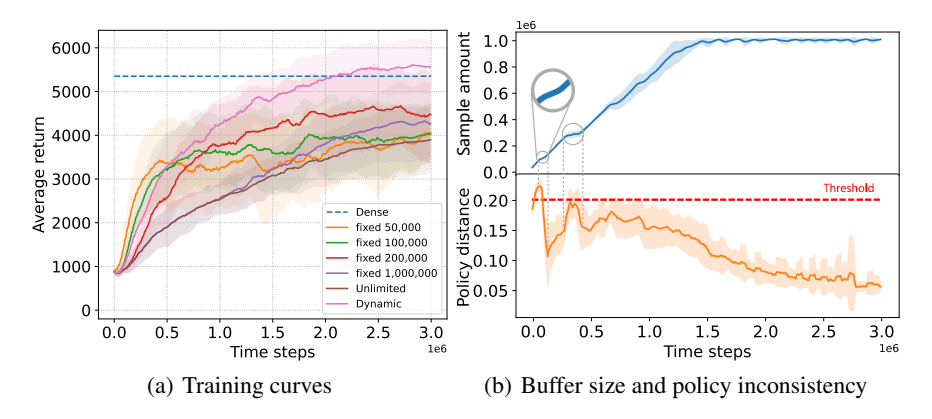


Figure 5: **Left**: Performance with different buffer schemes. Smaller buffer capacity benefits the performance in the early stage but may reduce the final performance. Our dynamic buffer outperforms the fixed capacity buffer. **Right**: Policy is updated quickly early on and leads to severe policy inconsistency. By dropping the oldest samples, our dynamic buffer scheme keeps the policy distance under the threshold. As the policy converges, the sample amount in the buffer also increases.

**Dynamic-capacity Buffer** We compare different replay buffer sizing schemes, including our dynamic scheme and using different fixed buffer capacities or an unlimited buffer. Figure 5(a) shows that our dynamic-capacity buffer performs best among all settings of the buffer. Using a smaller

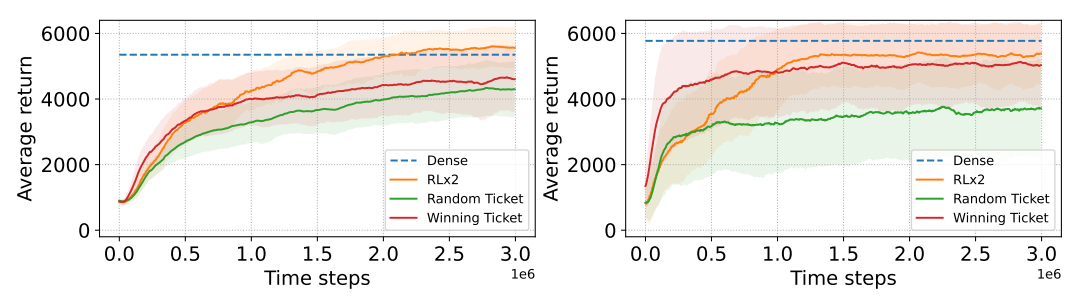
buffer results in higher sample efficiency in the early stage of training but fails in reaching high performance in the long term, whereas a large or even unlimited one may perform poorly in all stages. We also visualize in Figure 5(b) the sample amount and the proposed policy distance metric in Eq. (8) during training. The policy distance oscillates in the early stage as the policy evolves, but it is controlled and does not violate the threshold condition to effectively address the off-policyness issue. As the policy converges, the policy distance tends to decrease and converge.

### 5.3 Dynamic Topology vs. Winning Ticket

Previous subsections show that RLx2 can train an ultra-sparse model from scratch in DRL. This section compares the performance of using a dynamic topology (i.e., RLx2) versus only using a fixed winning ticket initialization to investigate the Lottery Ticket Hypothesis (LTH) [12]. Specifically, LTH demonstrates that a sparse network can be trained from scratch to reach the same performance as a dense one, if initialized with an appropriate mask [43], i.e., the "winning ticket." In particular, we compare the performance of random sparse initialization (fixed topology obtained randomly), winning ticket initialization (fixed topology obtained under RLx2 after training, with architecture visualization in Appendix), and random initialization with topology evolution (dynamic topology using RLx2) in both DRL learning and behavior cloning (BC).<sup>3</sup>

From Figure 6(a), we see that RLx2 with random initialization (orange curve) achieves the best performance, which is comparable with that under the original dense model. Although the winning ticket initialization (red curve) performs better than a random initialization (green curve), both without topology evolution, they lead to significant performance loss compared to RLx2, showing the necessity of topology evolution in DRL training from scratch.

On the other hand, Figure 6(b) shows that under BC, the winning ticket initialization and random initialization with topology evolution perform almost the same as the dense model, while the static random initialization performs worst. This indicates that an appropriate fixed initialization can indeed be sufficient to reach satisfactory performance in BC, which is intuitive since BC adopts a supervised learning approach and eliminates non-stationarity due to bootstrapping training, a result also observed in [41]. However, although the winning ticket initialization under BC achieves similar performance as RLx2, we emphasize that RLx2 uses a sparse topology throughout training, while BC-based methods rely on pre-training dense expert networks. As a result, RLx2 is able to accelerate training (in FLOPs) by a factor of  $7.5 \times -25 \times$  compared to BC.



(a) Rigging the Lottery Ticket in RL training

(b) Rigging the Lottery Ticket in behavior cloning

Figure 6: Comparison of different methods for training an DRL agent with a sparse network.

#### 6 Conclusion

This paper proposes a sparse training framework, RLx2, for off-policy reinforcement learning (RL). RLx2 utilizes gradient-based evolution to enable efficient topology exploration and establishes accurate value learning using multi-step TD targets and a dynamic-capacity replay buffer. RLx2 enables training an efficient DRL agent with minimal performance loss using an ultra-sparse network throughout and removes the need for pre-training dense networks. Our extensive experiments on RLx2 with TD3 and SAC demonstrate state-of-the-art sparse training performance, showing a  $7.5\times-20\times$  model compression with less than 3% performance degradation and up to  $20\times$  and  $50\times$  FLOPs reduction in training and inference, respectively.

<sup>&</sup>lt;sup>3</sup>In BC, the actor network is trained under the guidance of a well-trained expert, instead of the critic network.

# **Supplementary Materials**

A	Add	itional Details for Section 4	11
	A.1	Derivation of Eq. (6) in Section 4.2.1	11
	A.2	Algorithm of Dynamic-capacity Buffer in Section 4.2.2	11
В	Deta	ails of RLx2 with TD3 and SAC	11
C	Exp	erimental Details	14
	C.1	Hardware Setup	14
	C.2	Hyperparameter Settings for Reproduction	14
	C.3	Calculation of Model Size and FLOPs	14
	C.4	Training Curves of Comparative Evaluation in Section 5.1	17
	C.5	Supplementary Results for Ablation Study	18
	C.6	Supplementary Results for Investigation of the Lottery Ticket Hypothesis	18
	C.7	Visualization of Sparse Models	19

#### A Additional Details for Section 4

This section provides additional details for Section 4, including the derivation of Eq. (6) in Section 4.2.1, and the full algorithm of dynamic-capacity buffer in Section 4.2.2.

#### A.1 Derivation of Eq. (6) in Section 4.2.1

Denote  $p_{\pi}(s_{t+1}, a_{t+1}, \cdots, s_{t+n}, a_{t+n} | s_t, a_t)$  as the distribution of the trajectory starting from the current state  $s_t$  and action  $a_t$  under policy  $\pi$ . For simplicity, we use  $\mathbb{E}_{\pi}$  to denote  $\mathbb{E}_{(s_{t+1}, a_{t+1}, \cdots, s_{t+n}, a_{t+n}) \sim p_{\pi}(\cdot | s_t, a_t)}$ , and use  $\mathbb{E}_b$  to denote  $\mathbb{E}_{(s_{t+1}, a_{t+1}, \cdots, s_{t+n}, a_{t+n}) \sim p_b(\cdot | s_t, a_t)}$ , where  $\pi$  and b denote the current policy and the behavior policy, respectively.  $Q_{\pi}(s, a)$  denotes the Q function associated with policy  $\pi$  as defined in Eq. (1) in the manuscript, i.e.,  $Q_{\pi}(s, a) = \mathbb{E}_{\pi}\left[\sum_{i=t}^{T} \gamma^{i-t} r\left(s_i, a_i\right) | s_t = s, a_t = a\right]$ . Besides, we use  $\epsilon(s, a)$  to denote the network fitting error, i.e.,  $\epsilon(s, a) = Q(s, a; \theta) - Q_{\pi}(s, a)$ .

Subsequently, we have:

$$\mathbb{E}_{b}[\mathcal{T}_{n}(s_{t}, a_{t})] - Q_{\pi}(s_{t}, a_{t}) \\
= \mathbb{E}_{b}[\sum_{k=0}^{n-1} \gamma^{k} r_{t+k} + \gamma^{n} Q(s_{t+n}, \pi(s_{t+n}); \theta)] - \mathbb{E}_{\pi}[\sum_{k=0}^{n-1} \gamma^{k} r_{t+k} + \gamma^{n} Q_{\pi}(s_{t+n}, \pi(s_{t+n}))] \\
= \mathbb{E}_{b}[\sum_{k=0}^{n-1} \gamma^{k} r_{t+k} + \gamma^{n} Q(s_{t+n}, \pi(s_{t+n}); \theta)] - \mathbb{E}_{\pi}[\sum_{k=0}^{n-1} \gamma^{k} r_{t+k} + \gamma^{n} Q(s_{t+n}, \pi(s_{t+n}); \theta)] \\
+ \mathbb{E}_{\pi}[\gamma^{n}(Q(s_{t+n}, \pi(s_{t+n}); \theta) - Q_{\pi}(s_{t+n}, \pi(s_{t+n}))] \\
= (\mathbb{E}_{b}[\mathcal{T}_{n}(s_{t}, a_{t})] - \mathbb{E}_{\pi}[\mathcal{T}_{n}(s_{t}, a_{t})]) + \gamma^{n} \mathbb{E}_{\pi}[\epsilon(s_{t+n}, \pi(s_{t+n}))].$$

The first equality holds by definitions in Eq. (1) and Eq. (5) in the manuscript. The second equality holds by firstly adding and then subtracting the term  $\mathbb{E}_{\pi}[\gamma^n(Q(s_{t+n},a_{t+n};\theta))]$ . And the last equality holds by definitions of  $\mathcal{T}_n(s,a)$  and  $\epsilon(s,a)$ . This decomposition shows that the expected error consists of two parts, i.e., the network fitting error and the policy inconsistency error, which are well handled by our multi-step TD targets with dynamic-capacity buffer.

#### A.2 Algorithm of Dynamic-capacity Buffer in Section 4.2.2

Algorithm 2 presents our formal procedure for dynamically controlling the buffer capacity in Section 4.2.2. For each step, a new transition is inserted into the replay buffer. To avoid the problem of policy inconsistency, we check the buffer per  $\Delta_b$  steps and drop the oldest transitions if needed. Specifically, we first set a hard lower bound  $B_{\min}$  and a hard upper bound  $B_{\max}$  of the buffer capacity. (i) If the buffer size is below  $B_{\min}$ , we store all newly collected data samples. (ii) If the amount of buffered transitions has reached  $B_{\max}$ , the oldest transitions will be replaced by the latest transitions. (iii) When the buffer is in  $(B_{\min}, B_{\max})$ , for each time, we calculate the policy distance (defined in (8)) between the oldest behavior policy and the current policy, based on the oldest transitions stored in the buffer. Besides, if the policy distance exceeds the threshold  $D_0$ , the oldest transitions are discarded. And the full algorithm is given in Algorithm 2.

#### B Details of RLx2 with TD3 and SAC

In this section, we provide the pseudo-codes of instantiations of RLx2 on TD3 and SAC in Algorithm 3 and Algorithm 4, respectively. We emphasize that RLx2 is a general sparse training framework for off-policy DRL, and can be applied to training other DRL algorithms apart from TD3 and SAC, with sparse networks from scratch. Below, we first illustrate the critical steps of RLx2 in Algorithm 3, using TD3 as the base algorithm.

**Topology evolution** is performed in Lines 15-17 and Lines 20-22 in Algorithm 1. Specifically, we first calculate the sparsity of each layer according to the target sparsity of the total model at initialization. The sparsity of each layer is fixed during the training. And we use the Erdős–Rényi strategy, which is introduced in [26], to allocate the sparsity to each layer. For a sparse network with

#### Algorithm 2 Dynamic-Capacity Buffer for off-policy DRL

```
1: \pi: current policy
2: \mathcal{B}: Replay buffer at training step t
3: \Delta_b: Buffer checking interval
4: D_0: Non-consistency threshold
5: \rho: Shrinking ratio
6: B_{\min}, B_{\max}: Range of capacity
7: for each training step t do
        Interact with environment and store new transitions in B //Add new transitions into the buffer
9:
        Sample mini-batch from \mathcal{B}
10:
        Training with sampled data //Depend on the training algorithm
11:
        if t \mod \Delta_b = 0 //Check the buffer periodically then
12:
           if |\mathcal{B}| \in (B_{\min}, B_{\max}) //The buffer capacity is limited in certain range then
13:
              Batch of oldest transitions (s_i, a_i)
              if \mathcal{D}(\pi) > D_0 //Drop the oldest transitions if the policy distance exceeds the threshold then
14:
15:
                 \mathcal{B} \leftarrow \text{Drop ratio } \rho \text{ of oldest transitions in } \mathcal{B}
16:
              end if
17:
           end if
18:
        end if
19: end for
```

L layers, this strategy utilizes the equations below:

$$(1 - S) \sum_{l} I_{l}O_{l} = \sum_{l=1}^{L} (1 - S_{l})I_{l}O_{l},$$
$$1 - S_{l} = k \frac{I_{l} + O_{l}}{I_{l} * O_{l}},$$

where S is the target sparsity of the model,  $S_l$  is the sparsity of the l-th layer,  $I_l$  is the input dimensionality of the l-th layer,  $O_l$  is the output dimensionality of the l-th layer, and k is a constant. The motivation of this strategy is that a layer with more parameters contains more redundancy. As a result, it can be compressed with a higher sparsity. The topology evolution update is performed every  $\Delta_m$  time steps. Definitions of other hyperparameters related to topology evolution are listed in Algorithm 1 in the manuscript.

**Buffer capacity adjustment** is performed in Lines 7-9. This adjustment is conducted every  $\Delta_b$  steps, with detailed procedure shown in Algorithm 2.

Multi-step TD target is computed in Lines 10-13. We found that using a multi-step TD target in the early stage of training may result in poor performance because the policy may evolve quickly, which results in severe policy inconsistency. Thus, we start the multi-step TD target only when the number of training steps succeeds a pre-set threshold  $T_0$ . As mentioned in Section 4.2.1, the one-step TD target and multi-step TD target in TD3 are computed as:

$$\mathcal{T}_{1} = r_{t} + \gamma Q(s_{t+1}, \pi(s_{t+1}); \theta),$$

$$\mathcal{T}_{n} = \sum_{k=0}^{n-1} \gamma^{k} r_{t+k} + \gamma^{n} Q(s_{t+n}, \pi(s_{t+n}); \theta).$$
(9)

Note that the calculation of the multi-step TD target in SAC is slightly different from that in TD3. Specifically, the one-step TD target for SAC is computed as:

$$\mathcal{T}_1 = r_t + \gamma(Q(s_{t+1}, \tilde{a}_{t+1}; \theta) - \alpha \log \pi(\tilde{a}_{t+1}|s_{t+1})), \tag{10}$$

where  $\tilde{a}_{t+1} \sim \pi(\cdot|s_{t+1})$ , and the *n*-step TD target for SAC is computed by

$$\mathcal{T}_n = \sum_{k=0}^{n-1} \gamma^k r_t + \gamma^n Q(s_{t+n}, \tilde{a}_{t+n}; \theta) - \alpha \sum_{k=0}^{n-1} \gamma^{k+1} \log \pi(\tilde{a}_{t+k+1} | s_{t+k+1}), \tag{11}$$

where  $\tilde{a}_{t+k+1} \sim \pi(\cdot|s_{t+k+1}), k = 0, 1, \dots, n-1$ . Due to this difference, we will see later in Section C.3 that the resulting FLOPs are slightly different for TD3 and SAC.

Besides, Algorithm 4 also gives the detailed implementation of RLx2 with SAC, where topology evolution is performed in Lines 15-17 and Lines 20-22, buffer capacity adjustment is performed in Lines 7-9, and the multi-step TD target is computed in Lines 10-13.

#### Algorithm 3 RLx2-TD3

```
1: Initialize sparse critic network Q_{\theta_1}, Q_{\theta_2} and sparse actor network \pi_{\phi} with random parameters \theta_1, \theta_2, \phi and
      random masks M_{\theta_1}, M_{\theta_2}, M_{\phi} with determined sparsity S^{(c)}, S^{(a)}.

    θ₁ ← θ₁ ⊙ Mθ₁, θ₂ ← θ₂ ⊙ Mθ₂, φ ← φ ⊙ Mφ. //Start with a random sparse network
    Initialize target networks θ¹ ← θ₁, θ² ← θ₂, φ' ← φ. Initialize replay buffer β.

 4: for t = 1 to T do
          Select action with exploration noise a_t \sim \pi_{\phi}(s_t) + \epsilon, \epsilon \sim \mathcal{N}(0, \sigma) and observe reward r_t and new state
          Store transition tuple (s_t, a_t, r_t, s_{t+1}) in \mathcal{B}
 6:
 7:
          if t \bmod \Delta_b = 0 then
              Buffer capacity adjustment
 8:
 9:
          end if //Check the buffer periodically
10:
          Set N = 1 temporarily if t < T_0 //Delay to use N-step TD target
11:
          Sample mini-batch of B N-step transitions (s_i, a_i, r_i, s_{i+1}, a_{i+1}, \cdots, s_{i+N}) from B
12:
          \tilde{a} \leftarrow \pi_{\phi'}(s_{i+N}) + \epsilon, \epsilon \sim clip(\mathcal{N}(0, \tilde{\sigma}), -c, c)
          Calculate N-step TD target y \leftarrow \sum_{k=0}^{N-1} \gamma^k r_{i+k} + \gamma^N \min_{j=1,2} Q_{\theta'_j}(s_{i+N}, \tilde{a}) //N-step TD target
13:
          Update critic networks \theta_j \leftarrow \theta_j - \lambda \nabla_{\theta_j} \frac{1}{B} \sum (y - Q_{\theta_j}(s_i, a_i))^2 for j = 1, 2
14:
15:
          if t \mod \Delta_m = 0 then
16:
               Topology_Evolution(Q_{\theta_i}) for j = 1, 2
           end if //Update the mask of critic periodically
17:
          if t \mod d = 0 then
18:
               Update actor network \phi \leftarrow \phi - \lambda \nabla_{\phi} \left( -\frac{1}{B} \sum Q_{\theta_1}(s_i, a_i) \right)
19:
20:
              if t/d \mod \Delta_m = 0 then
21:
                   Topology_Evolution(\pi_{\phi})
22:
              end if //Update the mask of actor periodically
23:
              Update target networks:
              \theta_i' \leftarrow \tau \theta_i + (1 - \tau)\theta_i', \phi' \leftarrow \tau \phi + (1 - \tau)\phi',

\theta_i' \leftarrow \theta_i' \odot M_{\theta_i}, \phi' \leftarrow \phi' \odot M_{\phi} //Target networks are also sparsified with the same mask
           end if
24.
25: end for
```

#### Algorithm 4 RLx2-SAC

```
1: Initialize sparse critic network Q_{\theta_1}, Q_{\theta_2} and sparse actor network \pi_{\phi} with random parameters \theta_1, \theta_2, \phi and
       random masks M_{\theta_1}, M_{\theta_2}, M_{\phi} with determined sparsity S^{(c)}, S^{(a)}.
 2: \theta_1 \leftarrow \theta_1 \odot M_{\theta_1}, \theta_2 \leftarrow \tilde{\theta}_2 \odot M_{\theta_2}, \phi \leftarrow \phi \odot M_{\phi}. //Start with a random sparse network
  3: Initialize target networks \theta_1' \leftarrow \theta_1, \theta_2' \leftarrow \theta_2. Initialize replay buffer \mathcal{B}.
 4: for t = 1 to T do
            Select action a_t \sim \pi_{\phi}(s_t), and observe reward r_t and new state s_{t+1}
            Store transition tuple (s_t, a_t, r_t, s_{t+1}) in \mathcal{B}
 6:
 7:
            if t \mod \Delta_b = 0 then
 8:
                Buffer capacity adjustment
            end if //Check the buffer periodically
 9:
            Set N = 1 temporarily if t < T_0 //Delay to use N-step TD target
10:
            Sample mini-batch of B N-step transitions (s_i, a_i, r_i, s_{i+1}, a_{i+1}, \cdots, s_{i+N}) from \mathcal{B}
11:
           Sample inimication B N-step transitions (s_i, a_i, r_i, s_{i+1}, a_{i+1}, \cdots, s_{i+N}) from B \tilde{a}_{i+k+1} \sim \pi(\cdot|s_{i+k+1}), k = 0, 1, \cdots, N-1 Calculate N-step TD target (N)-step TD target y \leftarrow \sum_{k=0}^{N-1} \gamma^k r_{i+k} + \gamma^N \min_{j=1,2} Q_{\theta_j'}(s_{i+N}, \tilde{a}_{i+N}) - \alpha \sum_{k=0}^{N-1} \gamma^{k+1} \log \pi(\tilde{a}_{i+k+1}|s_{i+k+1}) Update critic networks \theta_j \leftarrow \theta_j - \lambda \nabla_{\theta_j} \frac{1}{B} \sum (y - Q_{\theta_j}(s_i, a_i))^2 for j = 1, 2
12:
13:
14:
15:
            if t \mod \Delta_m = 0 then
                 Topology_Evolution(Q_{\theta_j}) for j = 1, 2
16:
            end if //Update the mask of critic periodically
17:
18:
            Update actor network \phi \leftarrow \phi - \lambda \nabla_{\phi} \left( -\frac{1}{B} \sum \min_{j=1,2} Q_{\theta_j}(s_i, a_i) \right)
19:
            if t/d \mod \Delta_m = 0 then
                 Topology_Evolution(\pi_{\phi})
20:
21:
            end if //Update the mask of actor periodically
            Automating Entropy Adjustment: \alpha \leftarrow \alpha - \lambda \nabla_{\alpha} \frac{1}{B} \sum (-\alpha \log \pi(a_i|s_i) - \alpha \overline{\mathcal{H}})
22:
23:
            Update target networks:
            \theta_i' \leftarrow \tau \theta_i + (1 - \tau)\theta_i', \theta_i' \leftarrow \theta_i' \odot M_{\theta_i} //Target networks are also sparsified with the same mask
24: end for
```

### C Experimental Details

We provide more experimental details in this section, including the detailed experimental setup, the calculations of model size and FLOPs, and supplementary experiment results.

#### C.1 Hardware Setup

Our experiments are implemented with PyTorch [31] and run on 8x P100 GPUs. Each run needs 12 hours for TD3 and 2 days for SAC for three million steps. The code will be open-sourced upon publication of the paper.

#### C.2 Hyperparameter Settings for Reproduction

Table 4 presents detailed hyperparameters of RLx2-TD3 and RLx2-SAC in our experiments.

Category Hyperparameter Value **Optimizer** Adam Learning rate  $\lambda$  $3 \times 10^{-4}$ Discount factor  $\gamma$ 0.99 Number of hidden layers (all networks) 2 Number of hidden units per layer 256 Shared **Activation Function** ReLU Hyperparameters Batch size B256 Warmup steps 25000 Target update rate  $\tau$ 0.005 Initial mask update fraction  $\zeta_0$ 0.5 Mask update interval  $\Delta_m$ 10000 Buffer adjustment interval  $\Delta_b$ 10000 Buffer policy distance threshold  $D_0$ 0.2 Multi-step delay  $T_0$  $3 \times 10^{5}$ 2 Target update interval Actor update interval d2 Hyperparameters for RLx2-TD3 **Exploration policy**  $\mathcal{N}(0, 0, 1)$ Multi-step 3 Target update interval **Hyperparameters** Actor update interval d for RLx2-SAC Entropy target  $\overline{\mathcal{H}}$  $-\dim(\mathcal{A})$ 

Table 4: Hyperparameters of RLx2-TD3 and RLx2-SAC.

#### C.3 Calculation of Model Size and FLOPs

We present the details of calculating model sizes and FLOPs in this subsection, where focus on fully-connected layers since the networks used in our experiments are all Multilayer Perceptrons (MLPs). These calculations can be easily extended to convolutional layers or other architectures. Besides, we omit the offset term in fully-connected layers in our calculations.

2

Multi-step

#### C.3.1 Model Size

We first illustrate the calculation of model sizes, i.e., the total number of parameters in the model. Initially, for a sparse network with L fully-connected layers, we calculate the model size as:

$$M = \sum_{l=1}^{L} (1 - S_l) I_l O_l,$$

where  $S_l$  is the sparsity,  $I_l$  is the input dimensionality, and  $O_l$  is the output dimensionality of the l-th layer. Specifically, the "Total Size" column in Table 2 in the manuscript refers the model size including both actor and critic networks during training.

For both TD3 and SAC, double Q-learning is adopted, i.e., train two value networks concurrently. Besides, we also use target networks in our implementations as target critics for both TD3 and SAC, yet a target actor only for TD3. Thus, if we denote  $M_{\rm Actor}$  and  $M_{\rm Critic}$  as model sizes of actor and critic, respectively, the detailed calculation of model sizes can be obtained as shown in the second column of Table 5.

Table 5: FLOPs and model size for RLx2-TD3 and RLx2-SAC.

Algorithm	Model size	FLOPs (average of each iteration during training)	FLOPs (inference)
RLx2-TD3 RLx2-SAC	$ \begin{array}{ c c } 2M_{\rm Actor} + 4M_{\rm Critic} \\ M_{\rm Actor} + 4M_{\rm Critic} \end{array} $	$ \left  \begin{array}{l} \text{Batch\_Size} \times (2.5 \text{FLOPs}_{\text{Actor}} + 8.5 \text{FLOPs}_{\text{Critic}}) \\ \text{Batch\_Size} \times (5 \text{FLOPs}_{\text{Actor}} + 10 \text{FLOPs}_{\text{Critic}}) \end{array} \right  $	FLOPs <sub>Actor</sub> FLOPs <sub>Actor</sub>

#### C.3.2 FLOPs

Initially, for a sparse network with L fully-connected layer, the required FLOPs for a forward pass is competed as follows (also adopted in [10] and [28]):

$$FLOPs = \sum_{l=1}^{L} (1 - S_l)(2I_l - 1)O_l,$$
(12)

where  $S_l$  is the sparsity,  $I_l$  is the input dimensionality, and  $O_l$  is the output dimensionality of the l-th layer. Denote FLOPs<sub>Actor</sub> and FLOPs<sub>Critic</sub> as the FLOPs required in a forward pass of a single actor and critic network, respectively. The inference FLOPs is exactly FLOPs<sub>Actor</sub> as shown in the last column of Table 5. As for the training FLOPs, the calculation consisted of multiple forward and backward passes in several networks, which will be detailed below.

In particular, we compute the FLOPs needed for each training iteration. Besides, we omit the FLOPs of the following processes since they have little influence on the final result.

- (i) Interaction with the environment. Each time the agent decides an action to interact with the environment takes FLOPs as FLOPs<sub>Actor</sub>, which is much smaller than the FLOPs need for updating networks as shown in Table 5 since Batch Size  $\gg 1$ .
- (ii) Updating target networks. Every parameter in the networks is updated as  $\theta' \leftarrow \tau\theta + (1-\tau)\theta'$ . Thus, the number of FLOPs here is the same as the model size, which is also negligible.
- (iii) Topology evolution and buffer capacity adjustment. These two components are performed every 10000 steps. Formally speaking, the average FLOPs of topology evolution is give by Batch\_Size  $\times \frac{2\text{FLOPs}_{\text{Actor}}}{(1-S^{(a)})\Delta_m}$  for the actor, and Batch\_Size  $\times \frac{4\text{FLOPs}_{\text{Critic}}}{(1-S^{(c)})\Delta_m}$  for the critic, where  $S^{(a)}$  and  $S^{(c)}$  are the sparsity of actor and critic, respectively. The FLOPs of buffer capacity adjustment is  $8\text{Batch}\_\text{Size} \times \frac{\text{FLOPs}_{\text{Actor}}}{\Delta_b}$ , where  $8\text{Batch}\_\text{Size}$  is because that we use the oldest  $8\text{Batch}\_\text{Size}$  transitions to compute the policy distance. Thus, they are both negligible.

Therefore, we focus on the FLOPs of updating actor and critic. The average FLOPs of updating actor and critic can be given as:

$$FLOPs_{train} = FLOPs_{update\_critic} + \frac{1}{d}FLOPs_{update\_actor}, \tag{13}$$

where d is the actor update interval (2 for TD3 and 1 for SAC in our implementations). Next we calculate the FLOPs of updating actor and critic, i.e. FLOPs<sub>update\_critic</sub> and FLOPs<sub>update\_actor</sub>. We first focus on TD3, while that for SAC is similar.

#### **Training FLOPs Calculation in TD3**

(i) Critic FLOPs: Recall the way to update critic (two critics,  $\theta_1$  and  $\theta_2$ ) in TD3 is given by

$$\theta_j \leftarrow \theta_j - \lambda \nabla_{\theta_j} \frac{1}{B} \sum (\mathcal{T}_n - Q(s_i, a_i; \theta_j))^2,$$
 (14)

for j = 1, 2, where B is the batch size, n-step TD target

$$\mathcal{T}_{n} = \sum_{k=0}^{N-1} \gamma^{k} r_{i+k} + \gamma^{N} \min_{j=1,2} Q(s_{i+N}, \tilde{a}; \theta'_{j})$$

and  $\theta'_i$  refers to the target network.

Subsequently, we can compute the FLOPs of updating critic as:

$$FLOPs_{update \ critic} = FLOPs_{TD \ target} + FLOPs_{compute \ loss} + FLOPs_{backward \ pass}, \tag{15}$$

where FLOPs<sub>TD\_target</sub>, FLOPs<sub>compute\_loss</sub>, and FLOPs<sub>backward\_pass</sub> refer to the numbers of FLOPs in computing the TD targets in forward pass, loss function in forward pass, and gradients in backward pass (backward-propagation), respectively. By Eq. (14) we have:

$$FLOPs_{TD\_target} = Batch\_Size \times (FLOPs_{Actor} + 2FLOPs_{Critic}),$$
  

$$FLOPs_{compute\_loss} = Batch\_Size \times 2FLOPs_{Critic}.$$
(16)

For the FLOPs of gradients backward propagation, FLOPs<sub>backward\_pass</sub>, we compute it as two times the computational expense of the forward pass, widely adopted in existing literature [10], i.e.,

$$FLOPs_{backward\_pass} = Batch\_Size \times 2 \times 2FLOPs_{Critic}, \tag{17}$$

where the extra factor  $\underline{2}$  comes from the cost of double Q-learning.

Combining Eq. (15), Eq. (16), and Eq. (17), the FLOPs of updating critic in TD3 is:

$$FLOP_{s_{update \ critic}} = Batch\_Size \times (FLOP_{s_{Actor}} + 8FLOP_{s_{Critic}}). \tag{18}$$

(ii) Actor FLOPs: Recall the way to update actor (parameterized by  $\phi$ ) in TD3 is given by

$$\phi \leftarrow \phi - \lambda \nabla_{\phi} (-\frac{1}{B} \sum_{i} Q(s_i, a_i; \theta_1)),$$

where  $\theta_1$  refers to a critic network. Subsequently, we compute the FLOPs of updating actor as:

$$FLOPs_{update\_actor} = FLOPs_{compute\_loss} + FLOPs_{backward\_pass},$$
 (19)

and similar to the calculations of updating critic, we have:

$$FLOPs_{compute\_loss} = Batch\_Size \times (FLOPs_{Actor} + FLOPs_{Critic}),$$
  

$$FLOPs_{backward\_pass} = Batch\_Size \times 2FLOPs_{Actor}.$$
(20)

Combining Eq. (19), Eq. (19) and Eq. (20), the flops of updating actor in TD3 is:

$$FLOPs_{update\_actor} = Batch\_Size \times (3FLOPs_{Actor} + FLOPs_{Critic})$$
 (21)

#### **Training FLOPs Calculation in SAC**

(i) *Critic FLOPs*: Calculations of FLOPs for SAC are similar to that in TD3. The way to update the critic in SAC is:

$$\theta_j \leftarrow \theta_j - \lambda \nabla_{\theta_j} \frac{1}{B} \sum (\mathcal{T}_n - Q_{\theta_j}(s_i, a_i))^2$$

for j = 1, 2, where B is the batch size, n-step TD target

$$\mathcal{T}_n = \sum_{k=0}^{N-1} \gamma^k r_{i+k} + \gamma^N \min_{j=1,2} Q_{\theta'_j}(s_{i+N}, \tilde{a}_{i+N}) - \alpha \sum_{k=0}^{N-1} \gamma^{k+1} \log \pi(\tilde{a}_{i+k+1} | s_{i+k+1})$$

and  $\theta'_j$  refers to the target network. Note that the way to compute multi-step TD target in SAC is slightly different from which in TD3, we have:

$$FLOPs_{TD\_target} = Batch\_Size \times (2FLOPs_{Actor} + 2FLOPs_{Critic}). \tag{22}$$

Other terms for updating critic are the same as those in Eq. (15) for TD3. Thus, the FLOPs of updating critic in SAC can be computed by

$$FLOPs_{update\ critic} = Batch\_Size \times (2FLOPs_{Actor} + 8FLOPs_{Critic}). \tag{23}$$

(ii) Actor FLOPs: The way to update the actor in SAC is:

$$\phi \leftarrow \phi - \lambda \nabla_{\phi} \left( -\frac{1}{B} \sum \min_{j=1,2} Q_{\theta_j}(s_i, a_i) \right),$$

where  $\theta_j$  refers to a critic network. Subsequently, we have:

$$FLOPs_{compute\_loss} = Batch\_Size \times (FLOPs_{Actor} + 2FLOPs_{Critic}). \tag{24}$$

The backward pass FLOPs is the same as that in TD3, i.e.,

$$FLOPs_{backward\_pass} = Batch\_Size \times 2FLOPs_{Actor}.$$
 (25)

Thus, the FLOPs of updating the actor in SAC is:

$$FLOPs_{update\_actor} = Batch\_Size \times (3FLOPs_{Actor} + 2FLOPs_{Critic}). \tag{26}$$

#### C.4 Training Curves of Comparative Evaluation in Section 5.1

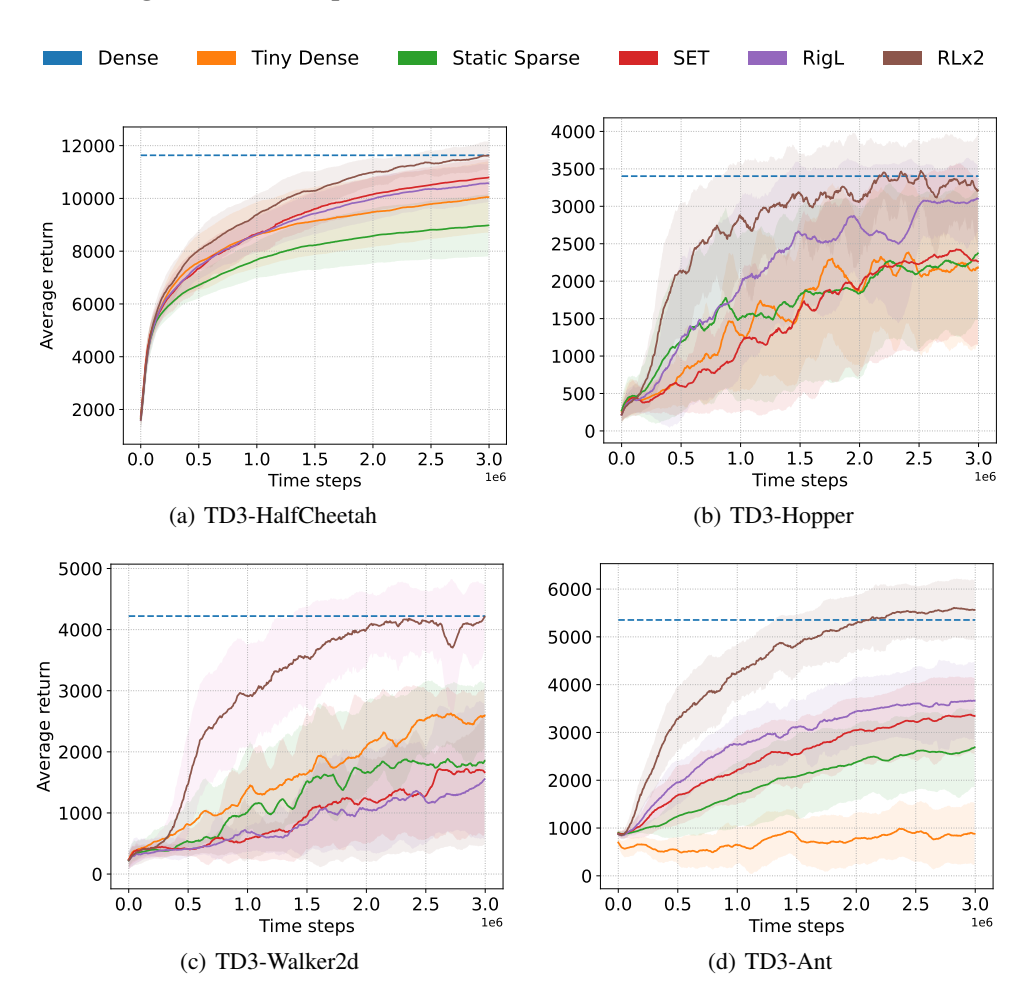


Figure 7: Training processes of RLx2-TD3 on four MuJoCo environments. The performance of each method is calculated as the average reward per episode over the last 30 evaluations of the training.

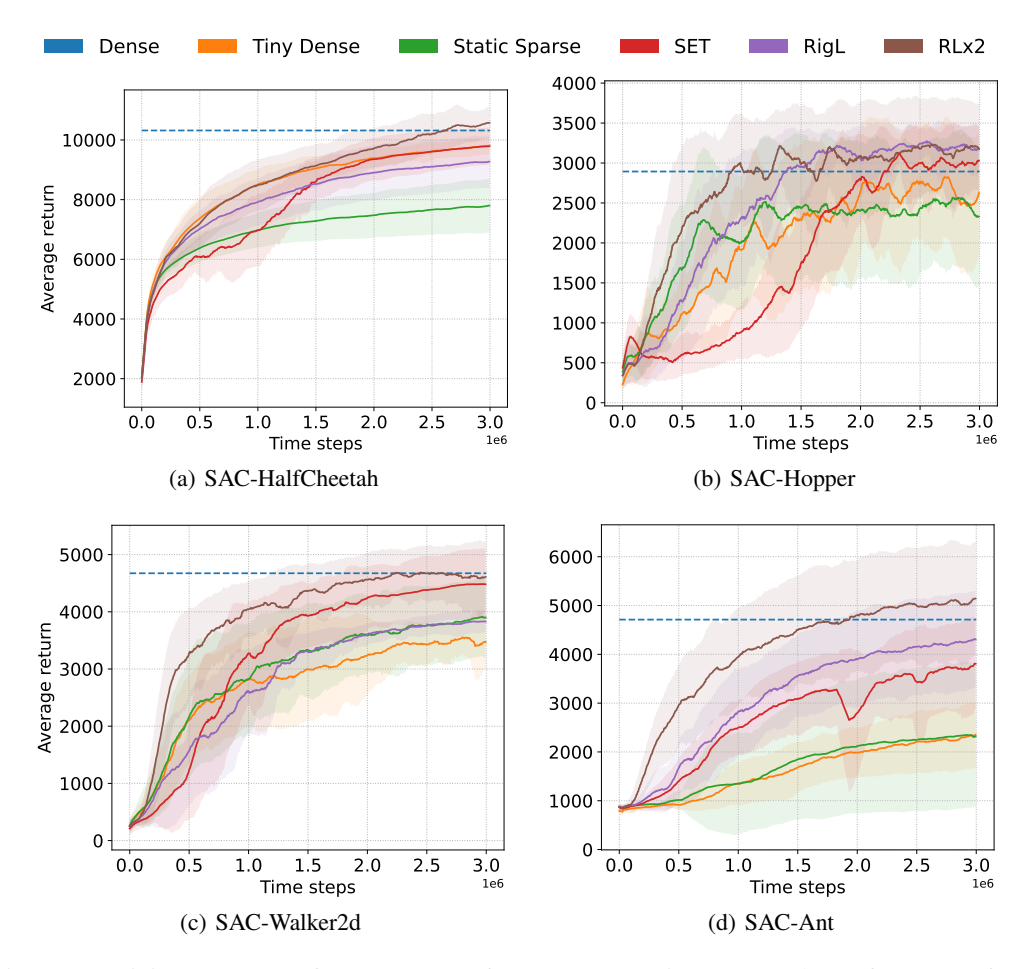


Figure 8: Training processes of RLx2-SAC on four MuJoCo environments. The performance of each method is calculated as the average reward per episode over the last 30 evaluations of the training.

#### C.5 Supplementary Results for Ablation Study

Table 6 shows the performance of four environments with different buffer capacities. Consistent with that presented in Section 5.2 in the manuscript, a buffer with either too small or too large capacity results in poor performance. Our dynamic buffer outperforms buffers with a fixed capacity.

Environment	Capacity $5 \times 10^4$	Capacity $1 \times 10^5$	Capacity $2 \times 10^5$	Capacity $1 \times 10^6$	Unlimited	Dynamic
HalfCheetah	84.5%	86.2%	93.7%	95.6%	88.2%	99.8%
Hopper	79.9%	94.1%	91.4%	94.5%	89.1%	97.0%
Walker2d	77.9%	94.7%	90.9%	90.2%	79.2%	<b>98.1</b> %
Ant	75.6%	75.1%	83.4%	80.0%	72.6%	103.9%

Table 6: RLx2-TD3 with different buffer capacity.

#### C.6 Supplementary Results for Investigation of the Lottery Ticket Hypothesis

We provide additional experiments with TD3 for investigation of the lottery ticket hypothesis (LTH) in the other three environments, including HalfCheetah-v3, Hopper-v3, and Walker2d-v3. As shown in Figure 9, winning tickets fail to achieve the same performance as the dynamic topology in the reinforcement learning setting, while they almost perform well similarly in the behavior cloning setting. This shows the necessity for reinforcement learning to adjust the network structure during the training process.

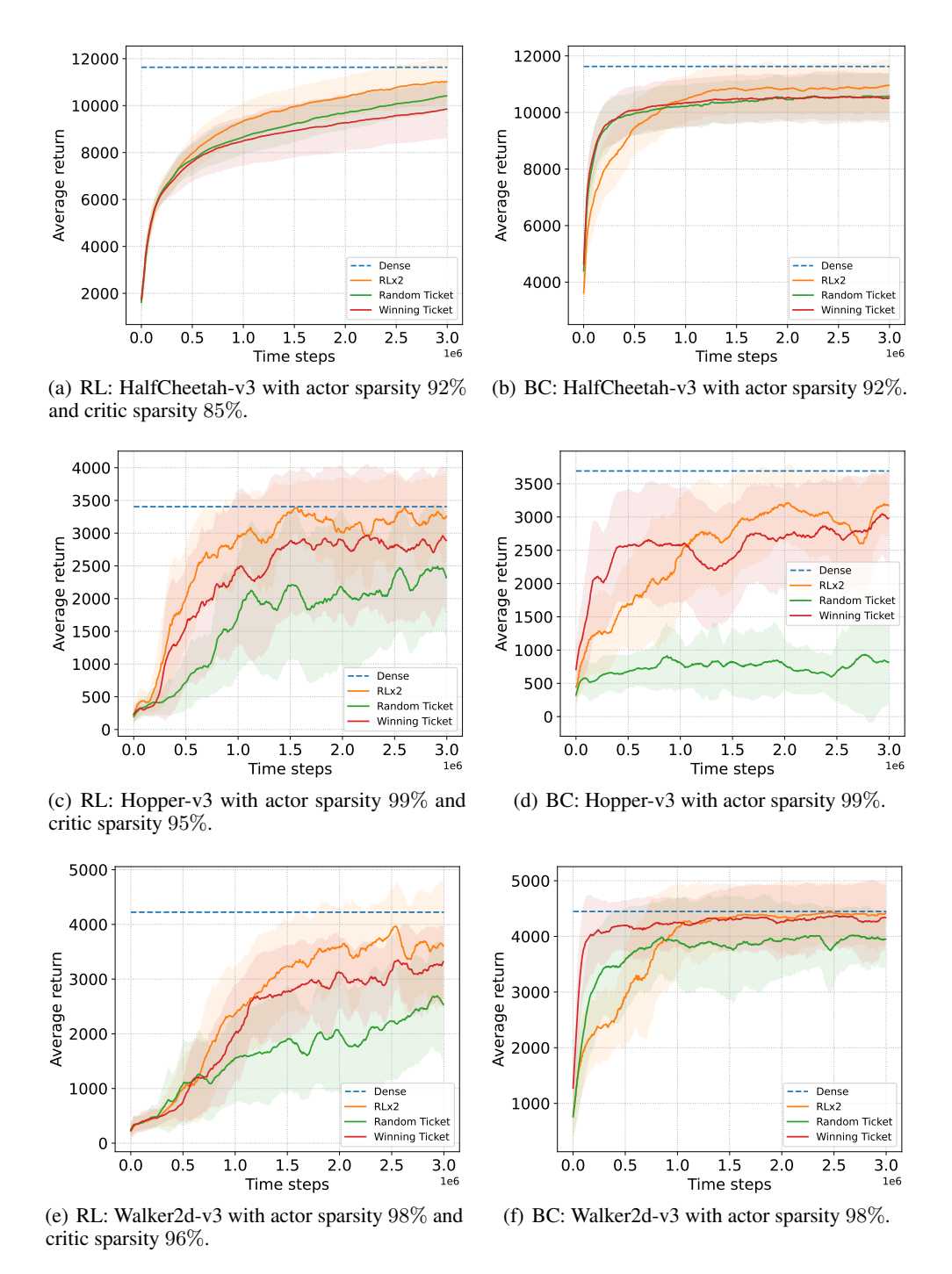


Figure 9: Comparisons of different methods for training a sparse DRL agent, where RLx2 is instantiated with TD3. Here, "RL" stands for the reinforcement learning setting, and "BC" stands for the behavior cloning setting.

#### C.7 Visualization of Sparse Models

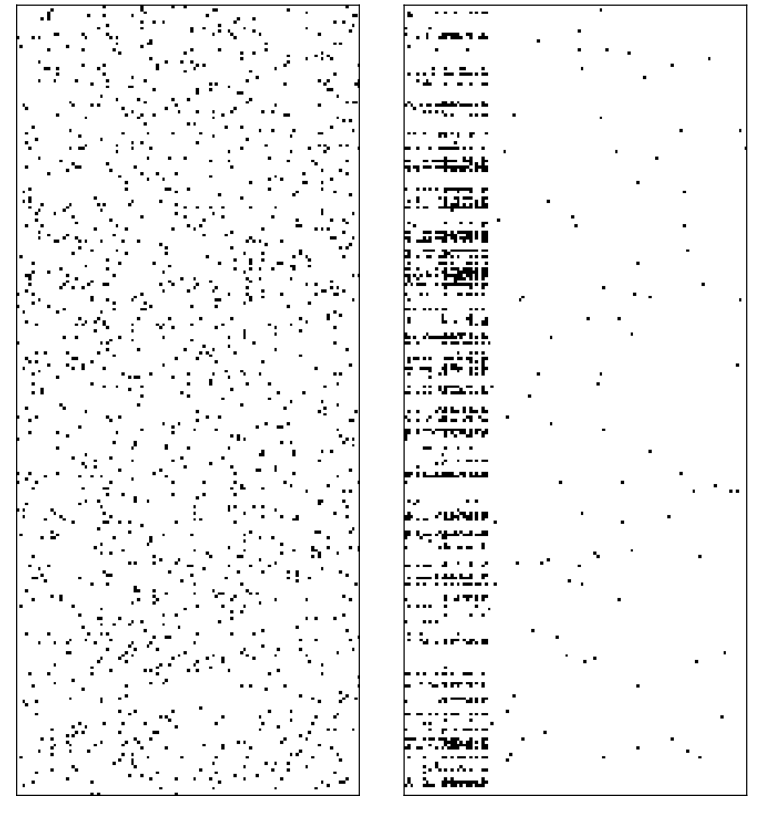
In this section, we show visualizations of the sparse networks obtained under RLx2 in our experiments. Note that each layer in the sparse network in our implementation is bound to a binary mask  $M_{\theta_l}$ , i.e.,  $\theta_l = \theta_l \odot M_{\theta_l}$  for the l-th layer. In the rest of this section, we investigate the property of the binary masks with visualization.

By visualizing the final mask after training, we find RLx2 drops redundant dimensions in raw inputs adaptively and efficiently. Specifically, Figure 10 shows the distribution of connections to each state dimension in Ant-v3. The figure shows that the resulting topology almost has no connections for input dimensions 28-118, and the connections heavily concentrate on the first 27 dimensions. This observation indicates that the topology evolution method drops redundant dimensions in raw inputs adaptively and efficiently. Besides, the observation is consistent with [41], which shows that by iterative magnitude training, input dimensions irrelevant to the task are pruned entirely to help yield a minimal task-relevant representation.



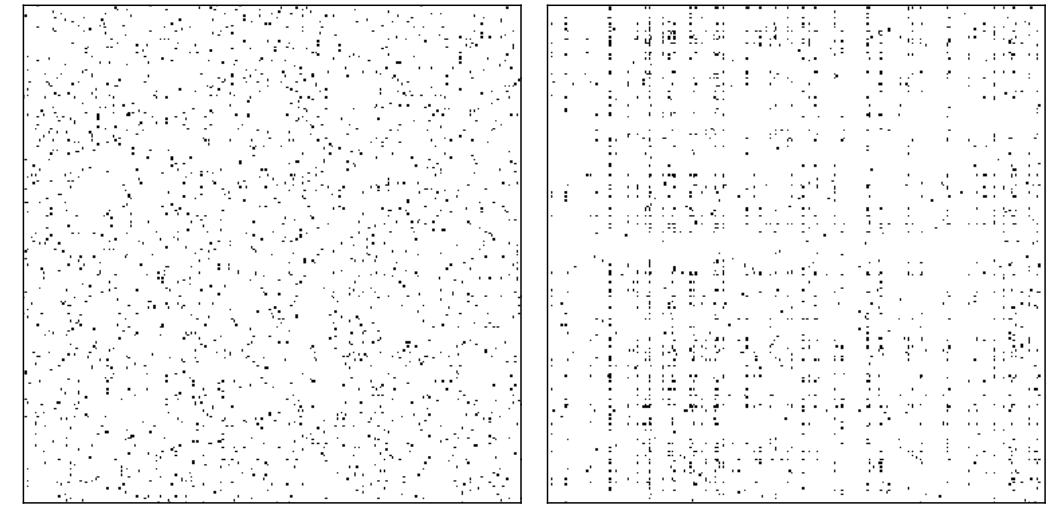
Figure 10: Distribution of connections to each state dimension in Ant-v3. Connections mainly concentrate on the first 27 dimensions.

Besides, visualizations of the raw binary masks (i.e., matrices with items representing neuron connections) of the actor in Ant-v3 are shown in Figure 11, where a black dot denotes an existing connection between the corresponding neurons, and a white point means there is no connection. As mentioned above, only very few connections are kept for the redundant input dimensions. We also find that the connections in the hidden layers tend to concentrate on a subset of neurons, showing that different neurons can play different roles in representations.



(a) Original mask of the first layer  $(256\times112)$ 

(b) Final mask of the first layer (256  $\times$  112)



(c) Original mask of the second layer  $(256 \times 256)$ 

(d) Final mask of the second layer  $(256 \times 256)$ 

(e) Original mask of the third layer  $(1 \times 256)$ 

## 

(f) Final mask of the third layer  $(1 \times 256)$ 

Figure 11: Visualization of the binary masks of the actor.

#### References

- [1] Samin Yeasar Arnob, Riyasat Ohib, Sergey Plis, and Doina Precup. Single-shot pruning for offline reinforcement learning. arXiv preprint arXiv:2112.15579, 2021.
- [2] Guillaume Bellec, David Kappel, Wolfgang Maass, and Robert Legenstein. Deep rewiring: Training very sparse deep networks. 2018.
- [3] Christopher Brix, Parnia Bahar, and Hermann Ney. Successfully applying the stabilized lottery ticket hypothesis to the transformer architecture. In *Proceedings of the 58th Annual Meeting of the Association for Computational Linguistics*, pages 3909–3915, 2020.
- [4] Tianlong Chen, Jonathan Frankle, Shiyu Chang, Sijia Liu, Yang Zhang, Zhangyang Wang, and Michael Carbin. The lottery ticket hypothesis for pre-trained bert networks. *Advances in neural information processing systems*, 33:15834–15846, 2020.
- [5] Tianlong Chen, Yongduo Sui, Xuxi Chen, Aston Zhang, and Zhangyang Wang. A unified lottery ticket hypothesis for graph neural networks. In *International Conference on Machine Learning*, pages 1695–1706. PMLR, 2021.
- [6] Jonas Degrave, Federico Felici, Jonas Buchli, Michael Neunert, Brendan Tracey, Francesco Carpanese, Timo Ewalds, Roland Hafner, Abbas Abdolmaleki, Diego de Las Casas, et al. Magnetic control of tokamak plasmas through deep reinforcement learning. *Nature*, 602(7897):414–419, 2022.
- [7] Shrey Desai, Hongyuan Zhan, and Ahmed Aly. Evaluating lottery tickets under distributional shifts. *arXiv preprint arXiv:1910.12708*, 2019.
- [8] Tim Dettmers and Luke Zettlemoyer. Sparse networks from scratch: Faster training without losing performance. *arXiv preprint arXiv:1907.04840*, 2019.
- [9] Xin Dong, Shangyu Chen, and Sinno Pan. Learning to prune deep neural networks via layer-wise optimal brain surgeon. *Advances in Neural Information Processing Systems*, 30, 2017.
- [10] Utku Evci, Trevor Gale, Jacob Menick, Pablo Samuel Castro, and Erich Elsen. Rigging the lottery: Making all tickets winners. In *International Conference on Machine Learning*, pages 2943–2952. PMLR, 2020.
- [11] William Fedus, Prajit Ramachandran, Rishabh Agarwal, Yoshua Bengio, Hugo Larochelle, Mark Rowland, and Will Dabney. Revisiting fundamentals of experience replay. In *International Conference on Machine Learning*, pages 3061–3071. PMLR, 2020.
- [12] Jonathan Frankle and Michael Carbin. The lottery ticket hypothesis: Finding sparse, trainable neural networks. In *International conference on learning representations*, 2019.
- [13] Scott Fujimoto, Herke Hoof, and David Meger. Addressing function approximation error in actor-critic methods. In *International conference on machine learning*, pages 1587–1596. PMLR, 2018.
- [14] Shixiang Gu, Ethan Holly, Timothy Lillicrap, and Sergey Levine. Deep reinforcement learning for robotic manipulation with asynchronous off-policy updates. In 2017 IEEE international conference on robotics and automation (ICRA), pages 3389–3396. IEEE, 2017.
- [15] Yiwen Guo, Anbang Yao, and Yurong Chen. Dynamic network surgery for efficient dnns. *Advances in neural information processing systems*, 29, 2016.
- [16] Tuomas Haarnoja, Aurick Zhou, Pieter Abbeel, and Sergey Levine. Soft actor-critic: Off-policy maximum entropy deep reinforcement learning with a stochastic actor. In *International conference on machine learning*, pages 1861–1870. PMLR, 2018.
- [17] Song Han, Huizi Mao, and William J Dally. Deep compression: Compressing deep neural networks with pruning, trained quantization and huffman coding. In *International conference on learning representations*, 2016.
- [18] Song Han, Jeff Pool, John Tran, and William Dally. Learning both weights and connections for efficient neural network. *Advances in neural information processing systems*, 28, 2015.
- [19] Matteo Hessel, Joseph Modayil, Hado Van Hasselt, Tom Schaul, Georg Ostrovski, Will Dabney, Dan Horgan, Bilal Piot, Mohammad Azar, and David Silver. Rainbow: Combining improvements in deep reinforcement learning. In *Thirty-second AAAI conference on artificial intelligence*, 2018.

- [20] Hengyuan Hu, Rui Peng, Yu-Wing Tai, and Chi-Keung Tang. Network trimming: A data-driven neuron pruning approach towards efficient deep architectures. arXiv preprint arXiv:1607.03250, 2016.
- [21] Maximilian Igl, Gregory Farquhar, Jelena Luketina, Wendelin Boehmer, and Shimon Whiteson. Transient non-stationarity and generalisation in deep reinforcement learning. In *International conference on learning representations*, 2021.
- [22] Juhyoung Lee, Sangyeob Kim, Sangjin Kim, Wooyoung Jo, and Hoi-Jun Yoo. Gst: Group-sparse training for accelerating deep reinforcement learning. arXiv preprint arXiv:2101.09650, 2021.
- [23] Namhoon Lee, Thalaiyasingam Ajanthan, and Philip HS Torr. Snip: Single-shot network pruning based on connection sensitivity. In *International conference on learning representations*, 2019.
- [24] Dor Livne and Kobi Cohen. Pops: Policy pruning and shrinking for deep reinforcement learning. *IEEE Journal of Selected Topics in Signal Processing*, 14(4):789–801, 2020.
- [25] Christos Louizos, Max Welling, and Diederik P Kingma. Learning sparse neural networks through  $l_{-}0$  regularization. In *International conference on learning representations*, 2018.
- [26] Decebal Constantin Mocanu, Elena Mocanu, Peter Stone, Phuong H Nguyen, Madeleine Gibescu, and Antonio Liotta. Scalable training of artificial neural networks with adaptive sparse connectivity inspired by network science. *Nature communications*, 9(1):1–12, 2018.
- [27] Dmitry Molchanov, Arsenii Ashukha, and Dmitry Vetrov. Variational dropout sparsifies deep neural networks. In *International Conference on Machine Learning*, pages 2498–2507. PMLR, 2017.
- [28] P Molchanov, S Tyree, T Karras, T Aila, and J Kautz. Pruning convolutional neural networks for resource efficient inference. In 5th International Conference on Learning Representations, ICLR 2017-Conference Track Proceedings, 2019.
- [29] Pavlo Molchanov, Arun Mallya, Stephen Tyree, Iuri Frosio, and Jan Kautz. Importance estimation for neural network pruning. In *Proceedings of the IEEE/CVF Conference on Computer Vision and Pattern Recognition*, pages 11264–11272, 2019.
- [30] Hesham Mostafa and Xin Wang. Parameter efficient training of deep convolutional neural networks by dynamic sparse reparameterization. In *International Conference on Machine Learning*, pages 4646–4655. PMLR, 2019.
- [31] Adam Paszke, Sam Gross, Soumith Chintala, Gregory Chanan, Edward Yang, Zachary DeVito, Zeming Lin, Alban Desmaison, Luca Antiga, and Adam Lerer. Automatic differentiation in pytorch. 2017.
- [32] Andrei A Rusu, Sergio Gomez Colmenarejo, Caglar Gulcehre, Guillaume Desjardins, James Kirkpatrick, Razvan Pascanu, Volodymyr Mnih, Koray Kavukcuoglu, and Raia Hadsell. Policy distillation. In *International conference on learning representations*, 2016.
- [33] Simon Schmitt, Jonathan J Hudson, Augustin Zidek, Simon Osindero, Carl Doersch, Wojciech M Czarnecki, Joel Z Leibo, Heinrich Kuttler, Andrew Zisserman, Karen Simonyan, et al. Kickstarting deep reinforcement learning. arXiv preprint arXiv:1803.03835, 2018.
- [34] David Silver, Guy Lever, Nicolas Heess, Thomas Degris, Daan Wierstra, and Martin Riedmiller. Deterministic policy gradient algorithms. In *International conference on machine learning*, pages 387–395. PMLR, 2014.
- [35] David Silver, Julian Schrittwieser, Karen Simonyan, Ioannis Antonoglou, Aja Huang, Arthur Guez, Thomas Hubert, Lucas Baker, Matthew Lai, Adrian Bolton, et al. Mastering the game of go without human knowledge. *nature*, 550(7676):354–359, 2017.
- [36] Ghada Sokar, Elena Mocanu, Decebal Constantin Mocanu, Mykola Pechenizkiy, and Peter Stone. Dynamic sparse training for deep reinforcement learning. arXiv preprint arXiv:2106.04217, 2021.
- [37] Suraj Srinivas, Akshayvarun Subramanya, and R Venkatesh Babu. Training sparse neural networks. In *Proceedings of the IEEE conference on computer vision and pattern recognition workshops*, pages 138–145, 2017.
- [38] Enzo Tartaglione, Skjalg Lepsøy, Attilio Fiandrotti, and Gianluca Francini. Learning sparse neural networks via sensitivity-driven regularization. *Advances in neural information processing systems*, 31, 2018.

- [39] Gerald Tesauro et al. Temporal difference learning and td-gammon. *Communications of the ACM*, 38(3):58–68, 1995.
- [40] Emanuel Todorov, Tom Erez, and Yuval Tassa. Mujoco: A physics engine for model-based control. In 2012 IEEE/RSJ international conference on intelligent robots and systems, pages 5026–5033. IEEE, 2012.
- [41] Marc Aurel Vischer, Robert Tjarko Lange, and Henning Sprekeler. On lottery tickets and minimal task representations in deep reinforcement learning. In *International conference on learning representations*, 2022.
- [42] Chaoqi Wang, Guodong Zhang, and Roger Grosse. Picking winning tickets before training by preserving gradient flow. *arXiv preprint arXiv:2002.07376*, 2020.
- [43] Haonan Yu, Sergey Edunov, Yuandong Tian, and Ari S Morcos. Playing the lottery with rewards and multiple languages: lottery tickets in rl and nlp. In *International conference on learning representations*, 2020.
- [44] Hongjie Zhang, Zhuocheng He, and Jing Li. Accelerating the deep reinforcement learning with neural network compression. In 2019 International Joint Conference on Neural Networks (IJCNN), pages 1–8. IEEE, 2019.
- [45] Michael Zhu and Suyog Gupta. To prune, or not to prune: exploring the efficacy of pruning for model compression. In *Workshop at international conference on learning representations*, 2018.